HHS Public Access

Author manuscript

Dev Cell. Author manuscript; available in PMC 2015 March 04.

Published in final edited form as:

Dev Cell. 2014 January 13; 28(1): 19–29. doi:10.1016/j.devcel.2013.11.012.

Structural Insights into Assembly and Regulation of the Plasma Membrane Phosphatidylinositol 4-Kinase Complex

Xudong Wu[1], **Richard J. Chi**[1], **Jeremy M. Baskin**[1,2], **Louise Lucast**[1,2], **Christopher G. Burd**[1], **Pietro De Camilli**[1,2], and **Karin M. Reinisch**[1,*]

[1]Department of Cell Biology, Yale School of Medicine, New Haven, CT 06520, USA

[2]Program in Cellular Neuroscience, Neurodegeneration, and Repair and Howard Hughes Medical Institute, Yale School of Medicine, New Haven, CT 06510, USA

SUMMARY

Plasma membrane PI4P helps determine the identity of this membrane and plays a key role in signal transduction as the precursor of $PI(4,5)P_2$ and its metabolites. Here, we report the atomic structure of the protein scaffold that is required for the plasma membrane localization and function of Stt4/PI4KIIIα, the PI 4-kinase responsible for this PI4P pool. Both proteins of the scaffold, Efr3 and YPP1/TTC7, are composed of α-helical repeats, which are arranged into a rod in Efr3 and a superhelix in Ypp1. A conserved basic patch in Efr3, which binds acidic phospholipids, anchors the complex to the plasma membrane. Stt4/PI4KIIIα is recruited by interacting with the Ypp1 C-terminal lobe, which also binds to unstructured regions in the Efr3 C terminus. Phosphorylation of this Efr3 region counteracts Ypp1 binding, thus providing a mechanism through which Stt4/PI4KIIIα recruitment, and thus a metabolic reaction of fundamental importance in cell physiology, can be regulated.

INTRODUCTION

Phosphoinositides, the membrane phospholipids that result from the reversible phosphorylation of the PtdIns inositol ring at the 3, 4, and 5 positions, play a wide variety of regulatory roles in cell physiology (Di Paolo and De Camilli, 2006). Via their cytosol-exposed head group, they control interactions of the bilayer with signaling, cytoskeletal, and trafficking proteins and with cytosolic regions of integral membrane proteins, thus regulating their activities. Because different phosphoinositides have different subcellular localization, they help to dictate specific properties of different membranes and thus are key determinants of membrane identity.

*Correspondence: karin.reinisch@yale.edu.

ACCESSION NUMBERS

Coordinates and structure factors for Efr3-N and Ypp1 have been deposited in the Protein Data Bank (IDs 4N5A and 4N5C).

SUPPLEMENTAL INFORMATION

Supplemental Information includes four figures and can be found with this article online at http://dx.doi.org/10.1016/j.devcel.2013.11.012.

At the plasma membrane, phosphoinositides play an especially important role because in addition to regulating constitutive functions of the membrane, they are also critical in the transduction of signals from the external world. Key players in signaling functions are PI4P and its downstream metabolites $PI(4,5)P_2$ and $PI(3,4,5)P_3$, as well as additional metabolites derived from $PI(4,5)P_2$ via the action of phospholipases and from $PI(3,4,5)P_3$ via the sequential action of inositol 5-phosphatases and 4-phosphatases. PI4P and $PI(4,5)P_2$ are key determinants of plasma membrane identity and participate in nearly every function associated with this membrane. $PI(3,4,5)P_3$ levels are very low under basal conditions but are dramatically elevated in the response to growth factor stimulation so that $PI(3,4,5)P_3$ is a major regulator of cell motility, protein synthesis, and cell proliferation and consequently plays key roles in the growth and metastatic dissemination of cancer cells.

Because phosphorylation of PtdIns at the 4 position to generate PI4P is the first reaction in the generation of all these signaling metabolites at the plasma membrane, this enzymatic reaction is particularly important. Thus, the PI 4-kinase complex that synthesizes PI4P has been implicated in a large number of cellular processes (Balla and Balla, 2006; D'Angelo et al., 2008). In yeast, where the complex has been most extensively studied, these include phosphatidylserine (PS) and sphingolipid homeostasis (Tabuchi et al., 2006; Trotter et al., 1998), actin dynamics (Foti et al., 2001), activation of the MAPK pathway (Audhya and Emr, 2002), and cell-cycle regulation (Muhua et al., 1998). In *Drosophila*, a mutation in a PI 4-kinase interaction partner leads to a paralytic defect at restrictive temperature (Huang et al., 2004), further underscoring the physiological importance of plasma membrane PI4P production.

The molecular mechanisms that underlie PI4P synthesis or its regulation are poorly understood. The PI 4-kinase that catalyzes conversion of PtdIns to PI4P at the plasma membrane, called PI4KIIIα in mammalian cells and Stt4 in yeast, is part of a protein complex that is well conserved in eukaryotes (Baird et al., 2008; Nakatsu et al., 2012). In addition to Stt4/PI4KIIIα, the complex comprises two other proteins: Efr3 (also known as "Rolling blackout," or RBO, in *Drosophila*) and a protein called Ypp1 in yeast (Baird et al., 2008) and TTC7 in mammals (Nakatsu et al., 2012). Both proteins are required for the recruitment of Stt4/PI4KIIIα to the plasma membrane and for its activity (Baird et al., 2008; Nakatsu et al., 2012), though the basis for plasma membrane targeting is unknown. In yeast, the PI4K complex is further organized into patches at the plasma membrane (Audhya and Emr, 2002; Baird et al., 2008). Efr3 is required for the plasma membrane association of the Stt4/PI4KIIIα complex (Baird et al., 2008; Nakatsu et al., 2012), and Ypp1/TTC7 interacts directly with both Efr3 and Stt4/PI4KIIIα (Baird et al., 2008; Nakatsu et al., 2012). These observations indicate that Efr3 and Ypp1 play key roles in the assembly of the Stt4/PI4KIIIα complex and its targeting to the plasma membrane. Interestingly, in human cells infected by hepatitis C virus (HCV), plasma membrane localization of PI4KIIIα is disrupted, and it is directed to the endoplasmic-reticulum-associated HCV replication compartment (Reiss et al., 2011). In addition, its activity is upregulated during viral infection, suggesting links among assembly, targeting, and activity of the complex. Beyond HCV, several other viruses require PI 4-kinase activity during viral infection, suggesting a general and fundamental connection between viral replication and PI4P metabolism (Altan-Bonnet and Balla, 2012).

The goal of this study was to understand the mechanisms that underlie the assembly and membrane targeting of the Stt4/PI4KIIIα complex and to obtain insights on how assembly at the plasma membrane may be regulated. To this end, we determined crystal structures of the proteins responsible for kinase localization, Efr3 and Ypp1/TTC7, and analyzed how they interact with each other, Stt4/PI4KIIIα, and membranes. We focused on the yeast proteins for the ease of genetics-based functional studies in this organism, which allowed validation of structural and biochemical findings. We found that an N-terminal portion of Efr3 (Efr3-N) and Ypp1 both are scaffold proteins comprising α-helical repeats. In Efr3-N, these repeats are folded into an elongated rod with a conserved basic patch at one end, and this patch mediates Efr3 membrane targeting, associating with acidic phospholipids as enriched in the plasma membrane. In Ypp1, HEAT-like repeats are arranged into a superhelix. Its C-terminal half interacts with both Stt4 and unstructured regions that form the C terminus of Efr3 (Efr3-C), thereby linking Efr3 and Stt4. The C-terminal portion of Efr3 is highly phosphorylated in vivo, and its phosphorylation abrogates the interaction with Ypp1, leading to Stt4 mislocalization and changes in PI4P levels in vivo. Our findings therefore indicate that assembly of the Stt4/PI4KIIIα complex at the plasma membrane, and hence its activity, can be regulated by Efr3 phosphorylation.

RESULTS AND DISCUSSION

Efr3-N Is a Rod of ARM- and HEAT-like Repeats

Although previous reports had proposed a transmembrane organization for Efr3 (Huang et al., 2004), Efr3 is a peripheral membrane protein (Nakatsu et al., 2012). Structure predictions suggested an N-terminal folded module followed by a disordered C-terminal region. Thus, in obtaining crystals, we focused on an N-terminal fragment from the *S. cerevisiae* protein (Efr3-$N_{8–562}$), and we obtained its structure at 3.2 Å resolution. Efr3-$N_{8–562}$ was recombinantly expressed in and purified from *E. coli* and crystallized in space group $P6_422$ with one molecule in the asymmetric unit. The single-wavelength anomalous dispersion method (SAD) with selenomethionine-substituted crystals was used for phasing. The final model, which includes residues 9–562 of Efr3-$N_{8–562}$ except for a disordered loop comprising residues 217–232, was refined to R_{work} = 23.11% and R_{free} = 25.56% with good geometry (Table 1 ; Figure S1 available online).

Efr3-$N_{8–562}$ is entirely α helical, with ARM- and HEAT-like repeats arranged into an almost straight ~120 Å long rod (Figure 1). Helices H1–H8 at the N terminus form a VHS domain, a mixture of ARM- and HEAT-like repeats, whereas the rest of Efr3-$N_{8–562}$ comprises primarily HEAT-like repeats.

Because functionally important surfaces are highly conserved in evolution, we analyzed and mapped sequence conservation onto the Efr3-$N_{8–562}$ structure (Ashkenazy et al., 2010) (Figure 1B). Two conserved surfaces are present. A small conserved patch near the middle of the Efr3-$N_{8–562}$ rod is formed by loops joining helices H11 and H12, H13 and H14, H15 and H16, and H17 and H18. Another prominent conserved patch at the N-terminal end of Efr3-$N_{8–562}$ is formed by helices H1-H2-H3 of the VHS domain at the tip of the rod.

It is worth noting that although the VHS domain sequence is the most conserved in Efr3, residues at the surface of H5 and H7 in the VHS domain are not well conserved. This surface functions in the recognition and binding of dileucine sorting signals in other characterized VHS domains (Misra et al., 2002; Shiba et al., 2002), but the lack of conservation in Efr3 suggests that its H5–H7 surface is unlikely to play a functionally important role, whether in peptide binding or otherwise.

We prepared yeast strains with mutant Efr3 proteins in which the conserved surfaces were altered for in vivo studies designed to assess the functional importance of these surfaces. In Efr3-3, residues in the prominent patch near the Efr3 N terminus were mutated (K12A, R46D, K49A, K52A, H67E, and R69A), whereas in Efr3-4 we altered the residues in the smaller conserved surface near the middle of Efr3 (V292D, Y296A, S336K, D339A, K371A, Q377A, and D380A) (Figure 1D). Wild-type or mutant Efr3, or C-terminally GFP-labeled versions of these proteins, were introduced into *S. cerevisiae* by the plasmid shuffling method (Sikorski and Boeke, 1991), replacing endogenous Efr3. Because Efr3 is essential (including under growth conditions used here), yeast strains harboring mutations that affect Efr3 function are expected to grow less well or be inviable. Indeed, we found that both Efr3-3 and Efr3-4 were growth impaired as compared to strains with wild-type Efr3 (Figure 2A). Efr3-3 mutations do not affect protein folding (Figure S2). Note, however, that because recombinant Efr3-4-N is prone to aggregation in vitro, we cannot entirely exclude that the Efr3-4 mutations could compromise protein folding or stability. Nevertheless, it is unlikely that the defect is severe in vivo because only surface residues were mutated, and, moreover, Efr3-4 rescues growth under standard conditions (30°C) and still localizes to the plasma membrane correctly (see below).

To directly assess the effect of Efr3 mutations on PI4K activity in vivo, we compared the cellular levels of PI4P and PI(4,5)P_2 and, as a control, PI3P in strains harboring wild-type or mutant proteins (Figure 2B). Strikingly, the levels of PI4P were reduced by ~30%–40% in the mutant strains, whereas the levels of PI3P were unaffected. Because the Stt4/PI4KIIIα complex is responsible for production of approximately half the cellular PI4P (Audhya et al., 2000; Nakatsu et al., 2012; Yoshida et al., 1994), this reduction indicates a severe defect in Stt4 function. Somewhat surprisingly, because PI4P is the precursor of PI(4,5)P_2, levels of PI(4,5)P_2 were not substantially altered. Nevertheless, this finding is consistent with previous studies in mammalian PI4KIIIα knockout cells, showing that cellular levels of PI(4,5)P_2 are maintained, likely as a result of compensatory production of PI(4,5)P_2 by another pathway (Nakatsu et al., 2012). These experiments confirm that both conserved surfaces in Efr3-$N_{8–562}$ are functionally important.

A Basic Surface Patch Is Required to Target Efr3 to the Plasma Membrane

Efr3 is proposed to target the Stt4/PI4KIIIα complex to the plasma membrane (Baird et al., 2008; Nakatsu et al., 2012), and we used fluorescence microscopy to monitor the effect of the mutations on the localization of Efr3-GFP constructs (Figure 2C). We found that mutations in the conserved patch near the middle of Efr3-$N_{8–562}$ (the Efr3-4 mutant) did not affect plasma membrane localization or localization to patches on the plasma membrane, suggesting that the middle patch does not play a role in the targeting of Efr3 itself. We have

not yet been able to ascribe a function to this conserved region of Efr3, but we speculate that it may represent a protein-protein interaction surface. Efr3-$N_{8–562}$ interacts with neither Ypp1 nor Stt4 in protein-protein interaction experiments (not shown). However, previously published immunoprecipitations suggest that interactors of the Stt4 complex remain to be identified (see Figure 5A in Audhya and Emr, 2002), and the patch near the middle of the Efr3-$N_{8–562}$ may mediate interactions with these proteins.

In contrast, mutations in the patch at the tip of the Efr3 rod (the Efr3-3 mutant) resulted in a near complete loss of plasma membrane localization, implicating the conserved patch at the Efr3 N terminus in membrane association. Because the basic charge of this surface (Figure 1C) suggests a potential interaction with the acidic cytosolic face of the plasma membrane, liposome binding assays were carried out to test whether Efr3-$N_{8–562}$ associates with negatively charged lipid bilayers directly. In an initial screen with different liposome compositions (Figures 2D and S3), we found that Efr3-$N_{8–562}$ associates efficiently with liposomes containing phosphoinositides (5%) but without a preference for a specific phosphoinositide. This result suggested that Efr3 may associate with acidic membranes via nonspecific electrostatic interactions. Consistent with this, Efr3 also bound avidly to liposomes containing physiologically relevant concentrations of PS (Figures 2E and S3). Additionally, Efr3-GFP localization to the plasma membrane is unaffected in *stt4*^{ts}, *mss4*^{ts}, and *pik1*^{ts} yeast backgrounds when cellular PI4P and PI(4,5)P_2 levels are depleted (not shown). Our data thus suggest that Efr3 recognizes the plasma membrane because of its enrichment in acidic phospholipids.

To further test this hypothesis, we performed liposome binding assays using Efr3-$N_{8–562}$ constructs harboring mutations in the basic patch: Efr3-N1 (K12A, R46D K49A, and K52A) and Efr3-N2 (H67E and R69A) (see Figure 1D). Liposome binding was markedly reduced for the basic patch mutant Efr3-N1 and not substantially affected for Efr3-N2 (Figures 2E and 2F) so that residues K12, R46, K49, and K52 define a conserved basic surface important for Efr3 plasma membrane association.

Unlike Efr3 of fungi, Efr3 of higher eukaryotes is N-terminally palmitoylated, and palmitoylation is required for plasma membrane association (Nakatsu et al., 2012). To investigate whether the basic patch, which is conserved in mammalian Efr3, provides an additional targeting activity, we performed in vivo localization experiments in mammalian cells similar to those described above for yeast. Basic patch mutations analogous to those in yeast Efr3-3 were generated in murine EFR3A-GFP (K50E, R53A, R61E, R68E, and R70E), and GFP fusions of wild-type and mutant Efr3 were expressed in HeLa cells. Whereas wild-type EFR3A-GFP localized to the plasma membrane, as reported in (Nakatsu et al., 2012), the EFR3A mutant mislocalized to intracellular compartments tentatively identified as endosomal compartments because of colocalization with a PI3P binding probe (mRFP-$FYVE_{Hrs}$ domain) (Figure 2G). Thus, the basic patch of mammalian Efr3 is required for correct localization to the plasma membrane.

Ypp1 Is a Superhelix of HEAT-like Repeats

Ypp1 from *S. cerevisiae* was recombinantly expressed in and purified from *E. coli* and crystallized in space group P1 with eight copies of Ypp1 in the unit cell. To obtain

diffraction quality crystals, ten residues at both the N terminus and in a poorly conserved loop (residues 732–741) were deleted in the crystallization construct. We determined the structure of the selenomethionine-substituted protein at 3.25 Å resolution by a combination of the SAD and molecular replacement methods, as described in more detail in the Experimental Procedures section. The N-terminal portion of Ypp1 (Ypp1-$N_{11–446}$, encompassing residues 11–446), for which we had independently determined the structure, was used as the search model in molecular replacement. We were able to model all eight Ypp1 copies within the unit cell. The most complete Ypp1 structure comprises residues 12–817, except for disordered loops spanning residues 131–134, 470–483, 714–741, and 788–790. Residues in several additional loops (residues 608–617, 661–666, and 680–683) could not be modeled in some of the other Ypp1 molecules within the unit cell. The structure was refined to R_{work} = 23.98% and R_{free} = 27.72% with good geometry (Table 1; Figure S1).

Ypp1 forms a dumbbell-like structure ~95 Å long and ~45 Å in diameter. Like Efr3-$N_{8–562}$, it consists primarily of HEAT-like repeats (helices H1–H34), in this case arranged into a superhelix (Figure 3) rather than a rod. The very C terminus (residues 806–817 marked by * in Figure 3) is inserted into the center of the Ypp1 superhelix. As has been observed in other superhelical proteins (Conti et al., 2006), Ypp1 is inherently flexible with conformational differences among independent copies in the crystal (Figure S4). Nevertheless, the first 500 residues superimpose well, with root-mean-square deviations (rmsd) in the carbon-alpha positions ranging from 0.33 Å to 0.43 Å. The superposition is poorer at the C-terminal end (residues 501–817), and the rmsd values are higher, between 0.30 Å and 0.73 Å.

To identify functionally important surfaces, we analyzed and mapped sequence conservation onto the Ypp1 structure (Figure 3B) (Ashkenazy et al., 2010). The C-terminal half of Ypp1 is generally well conserved, and there are several prominent conserved surfaces in this portion of the protein, whereas conservation is poorer in Ypp1-$N_{11–446}$, which has only a single conserved surface. None of these surfaces are basic, suggesting that Ypp1 does not interact directly with the acidic plasma membrane. Most likely, the conserved surfaces mediate interactions with other complex members or binding partners of the Stt4 complex, as explored below.

To assess the functional importance of the conserved surfaces, we generated Ypp1 constructs with mutations in the N-terminal conserved surface (Ypp1-δN: F255A, F303A, Q304A, and N342A) or with C-terminal deletions (Δ447–817, Δ726–817, and Δ806–817) and tested whether these constructs rescued Ypp1 null yeast strains. Ypp1-δN strains have a growth defect at restrictive temperature but are nevertheless able to rescue Ypp1 null alleles (Figure 3C). In contrast, the Ypp1 constructs with C-terminal deletions were not able to rescue Ypp1 null strains, suggesting that the C-terminal portion of Ypp1 is critical for function (Figure 3C), as explored further below.

Ypp1 Binds Stt4 via Its C-Terminal Lobe

Ypp1 binds both Stt4 and Efr3, thereby localizing Stt4 to the plasma membrane (Baird et al., 2008). We confirmed and further characterized the interaction between Ypp1 and Stt4, first using size-exclusion chromatography with purified recombinant proteins to estimate the stoichiometry of the Ypp1:Stt4 assembly (Figure 4A). Hexahistidine-tagged Ypp1 by itself

elutes as a monomer, but when it was mixed with FLAG-tagged Stt4 to allow for complex formation, it elutes in a fraction corresponding to an ~440 kDa globular protein. The elution profile suggests a 1:1, 1:2, or 2:1 Stt4:Ypp1 ratio and does not support that Stt4/Ypp1 complexes associate into larger arrays as previously proposed (Baird et al., 2008).

Next, to determine which portion of Ypp1 mediates the interaction with Stt4, we used pull-down experiments with glutathione-S-transferase (GST)-tagged Ypp1 constructs as the "bait" and FLAG-tagged Stt4 as the "prey." FLAG-tagged Stt4 was expressed in HEK293T cells, and lysates from these cells were used as starting material for the pull-down. Stt4 was retained by the Ypp1 crystallization construct (residues 11–817) and to a lesser extent by the C-terminal truncation construct Ypp1$_{11–725}$-ΔC, lacking helices H32–H34 and the C-terminal peptide (Figure 4B). In contrast, Ypp1-N$_{11–446}$ and the GST-only control did not retain Stt4. Thus, the interaction with Stt4 is most likely mediated by one or more of the highly conserved surfaces in the C-terminal half of Ypp1. We were unable to obtain soluble C-terminal Ypp1 fragments and therefore could not test for interactions between these and Stt4.

Interactions between C-Terminal Portions of Ypp1 and Efr3 Are Required for Stt4 Plasma Membrane Recruitment

We also used biochemical experiments to determine how Efr3 and Ypp1 interact. In these experiments GST-Efr3 constructs were used to pull down purified Ypp1 (residues 11–817). No interaction was detected between the Efr3-N$_{8–562}$ fragment used for crystallization and Ypp1, as expected from a previous report that Ypp1 binds the C-terminal half of Efr3 (residues 340–782) (Baird et al., 2008). Because this C-terminal region of Efr3 is predicted to be mostly random coil, it was subdivided into three smaller fragments (residues 353–650, 651–730, and 731–782), which were used as GST baits to more narrowly identify the binding site for Ypp1. We found that Ypp1 interacts with Efr3-C$_{651–730}$, but not with other fragments tested (Figure 4C). Additionally, we found that Ypp1-N$_{11–446}$ does not bind Efr3-C$_{651–730}$ (Figure 4D), strongly suggesting that the conserved surface patches in the C-terminal half of Ypp1 mediate interactions with both Efr3 and Stt4. Although the conserved surface at the Ypp1 N terminus is also likely to be a protein-protein interaction surface, we have not yet identified an interaction partner for it.

To probe the importance of the Efr3 C-terminal region for Stt4-complex function in living cells, we generated yeast strains in which endogenous Efr3 was replaced by a C-terminally truncated version of the protein, Efr3-ΔC$_{1–650}$, or its GFP-tagged form. Growth of the Efr3-ΔC$_{1–650}$ mutant was impaired (Figure 2A), and cellular PI4P levels were significantly reduced (by ~30%) (Figure 2B), indicating an important role for the C-terminal region of Efr3 in Stt4-complex function in vivo. As assessed by fluorescence microscopy, GFP-tagged Efr3-ΔC$_{1–650}$ localized to the plasma membrane, consistent with a role of its N-terminal basic patch in this localization (Figure 5A). Interestingly, however, it was more diffusely distributed along the membrane than the wild-type protein, suggestive of a role for Efr3 in the organization of patches. Importantly, ectopically expressed GFP-Stt4 had an entirely cytosolic distribution in strains expressing Efr3-ΔC$_{1–650}$, whereas it was localized to the plasma membrane and in patches in the presence of wild-type Efr3 (Figure 5B). These

experiments corroborate a model according to which the assembly of the Stt4 complex at the plasma membrane requires binding of the C-terminal region of Efr3 (residues 651–782) to Ypp1.

Phosphorylation of the Efr3 C Terminus Modulates Stt4 Complex Assembly

A variety of cellular stresses result in increased production of PI4P by Stt4 (Audhya and Emr, 2002; Jesch et al., 2010), leading to the proposal that Stt4 complex activity is regulated. Interestingly, database searches (http://www.phosphogrid.org) revealed that the poorly structured C-terminal tail of Efr3 is heavily phosphorylated, with more than 20 annotated phosphorylation sites. Four of these (S681, S684, T687, and T690) are in the highly conserved region in Efr3 containing the binding site for Ypp1. To test whether phosphorylation of these residues affects the Efr3/Ypp1 interaction, pull-down experiments similar to those described earlier were repeated with GST-Efr3$_{651–730}$ constructs in which either the serine or threonine residues were replaced by glutamate, a mimetic for their phosphorylated form. We found that either double mutation (S681E/S684E or T687E/T690E) substantially weakens the interaction between Ypp1 and Efr3-C$_{651–730}$ (Figure 5C), supporting the notion that Efr3 phosphorylation interferes with the Ypp1/Efr3 interaction. As Efr3 recruits Ypp1 to the membrane, which in turn recruits Stt4, abrogation of the Ypp1/Efr3 interaction is expected to interfere with Stt4 activity at the plasma membrane. That is, our result predicts that Efr3 phosphorylation modulates Stt4 complex assembly and activity.

To test this hypothesis directly, in vivo experiments were carried out. We generated an Efr3 mutant, Efr3-4×Glu, in which S681, S684, T687, and T690 at the C terminus were altered to glutamate, and expressed it as the sole copy of Efr3 in the cell. Efr3-4×Glu-GFP localized to the plasma membrane, and its distribution phenocopied that of Efr3-ΔC (Figure 5A). When GFP-Stt4 was expressed in these cells, a large fraction of Stt4 was observed in the cytosol (Figure 5B), and cellular PI4P levels were reduced by ~10% (Figure 5D). Although the reduction in PI4P level was more modest than that observed with the Efr3-ΔC mutant (~30%), it nevertheless supports the idea that Efr3-C phosphorylation partially disrupts a major Ypp1/Stt4 binding site on Efr3. The phosphorylation of other sites in the C-terminal region of Efr3 may also contribute to complex assembly or disassembly. Thus, our findings suggest that one mechanism by which Stt4/PI4KIIIα complex activity can be modulated is by regulating complex assembly via phosphorylation of the Efr3-C terminus.

Concluding Remarks

This study elucidates the mechanisms underlying Stt4/PI4KIIIα recruitment to the plasma membrane and provides insight regarding the regulation of this important complex (Figure 6). We have shown how the α-helical repeat proteins Efr3 and Ypp1 form a scaffold that serves in Stt4/PI4KIIIα recruitment, identifying a basic surface at one end of the Efr3-N rod required for Efr3 plasma membrane association and thus for Stt4 enzymatic action at the membrane. Further, we found that the unstructured C-terminal portion of Efr3 interacts with the C-terminal half of Ypp1 to localize Ypp1 and with it Stt4 to the plasma membrane. This interaction is attenuated by Efr3 phosphorylation, providing a mechanism by which to modulate Stt4/PI4KIIIα complex assembly and activity. It will be particularly interesting to

determine whether HCV intervenesin this mechanism to relocalize PI4KIIIα to the HCV replication compartment.

An intriguing feature of the yeast Stt4 complex not yet addressed is that it is not distributed uniformly along the plasma membrane but instead localizes to patches. How such patches form is unclear. It has been proposed that Ypp1 and Stt4 oligomerize, resulting in a crosslinked network (Baird et al., 2008). Our data, however, suggest that Ypp1 and Stt4 form a 1:1 or 1:2 heterodimer so that Ypp1-Stt4 interactions are unlikely to scaffold patch formation. Multimerization may be possible, however, through Efr3. Its C terminus is predicted to be mostly unstructured, and it could accommodate binding sites along its length (over 200 amino acids), making it well suited as a crosslink. Nevertheless, we favor the explanation that patches form because Stt4 complexes interact with lipid or protein-based microdomains, which are themselves enriched at particular sites along the plasma membrane. It has been suggested that Stt4 complexes form near endoplasmic reticulum-plasma membrane contact sites (Baird et al., 2008), and perhaps Stt4 complexes interact with protein residents of these sites. Whether patch formation is required for Stt4 function in yeast and whether the mammalian PI4KIIIα complex also forms patches remain open questions.

In conclusion, our work here is an important step in understanding the architecture and regulation of the Stt4/PI4KIIIα complex, and it provides a structural-biochemical framework that will be invaluable in guiding further investigations of an intricate enzyme complex.

EXPERIMENTAL PROCEDURES

Cloning

Coding sequences for Efr3-N (residues 8–562) and Ypp1-$N_{11–446}$ (residues 11–446) were cloned into a modified PET28 vector, which introduces an N-terminal dodeca-histidine-SUMO tag. Sequences for full-length $Ypp1_{11–817}$ as well as $Ypp1_{11–817(\Delta 732–741)}$, a loop deletion construct missing residues 732–741, Ypp1-$N_{11–446}$, and $Ypp11_{11–725}$ were cloned into a modified pCDF vector, which has an N-terminal GST tag followed by a Prescission protease cleavage site. Sequences for an N-terminally hexahistine-tagged version of $Ypp1_{11–817}$ for size-exclusion chromatography (in Figure 4) were cloned into the same pCDF vector, as were C-terminal fragments of Efr3 for pull-down experiments. We made mutations in Efr3 and Ypp1 using the QuikChange site-directed mutagenesis kit (Agilent Technologies).

Protein Expression

Plasmids containing the coding sequences for the Efr3 and Ypp1 constructs were transformed into *E. coli* BL21(DE3) cells. The cells were grown to an optical density (OD_{600}) of ~0.7 at 37°C, and then shifted to 18°C, and protein expression was induced by addition of 0.5 mM isopropylthio-β-galactosidase. The cells were harvested 20 hr after induction; transferred to lysis buffer (20 mM Tris[pH 8.0 at 21°C], 500mM NaCl, 1 mm TCEP, and 20 mM imidazole) supplemented with protease inhibitors (Complete EDTA-free,

from Roche), DnaseI (Sigma), and lysozyme (American Bioanalytical); and lysed using a cell disruptor (Avestin).

Purification

Efr3-N and Ypp1-N were isolated using Ni-NTA resin (QIAGEN). After elution, we cleaved off the his_{12}-SUMO tags with SUMO protease. Uncleaved protein was removed by passing the sample over Ni-NTA resin a second time and collecting the flow through. Protein was further purified by size-exclusion chromatography (Superdex200; GE Healthcare) and concentrated to ~10 mg/ml. The buffer for Efr3-N contains 20 mM Tris (pH 8.0 at 21 °C), 800 mM NaCl, and 2.5 mM Tris(2-carboxyethyl)phosphine (TCEP); the buffer for Ypp1-N was identical, except in its salt concentration (150 mM).

$Ypp1_{11–817}$, $Ypp1_{11–817(\Delta732–741)}$, and $Ypp1_{11–725}$ were bound to Glutathione-S-Sepharose 4B resin (GE Healthcare). Their GST tags were removed and the proteins eluted from the resin by cleavage with Prescission protease. Proteins were further purified by size-exclusion chromatography in buffer containing 20 mM Tris (pH 8.0 at 21 °C), 250 mM NaCl, and 2.5 mM TCEP, and then concentrated to ~5 mg/ml.

GST-tagged fragments of Efr3 and Ypp1 for the protein-protein interaction experiments were eluted from the Glutathione-S-Sepharose resin using glutathione and concentrated. During concentration, buffer was exchanged to one containing 20 mM HEPES (pH 7.4), 140 mM NaCl, and 0.5 mM TCEP.

Selenomethionine-substituted proteins for structure determination were prepared similarly to native proteins, according to Doublie, 1997.

Crystallization

Crystals of selenomethionine-substituted Efr3-N (residues 8–562) were grown by the hanging drop method at 21 °C by mixing 1.35 μl each of protein solution and mother liquor (0.08 M sodium cacodylate [pH 6.5], 0.16 M calcium acetate, 11.5% polyethylene glycol [PEG] 8,000, and 20% glycerol) and 0.3 μl of 0.1 M EDTA. These crystals belong to space group $P6_422$ (a = b = 136.37 Å, and c = 141.14 Å) with one molecule of Efr3-N in the asymmetric unit.

Crystals of selenomethionine-substituted Ypp1-N were obtained at 4°C using a 1:1 ratio of protein and well solution (0.1 M sodium acetate [pH 5.0] and 1.5 M ammonium tartrate). The crystals belong to space group $P2_12_12_1$ (a = 102.35 Å, b = 129.20 Å, and c = 185.45 Å) with four molecules of Ypp1-N in the asymmetric unit.

Crystals of selenomethionine-substituted $Ypp1_{11–817(\Delta732–741)}$ were grown at 16°C by mixing equal volumes of protein and well solution (0.1 Bis-Tris propane [pH 7.5], 0.2 M sodium bromide, 19% PEG 3,350, and 20 mM taurine). The crystals belong to space group P1 (a = 97.55 Å, b = 136.65 Å, and c = 154.125 Å; α = 76.69°C, β = 85.67°C, and γ = 72.74°C), with eight molecules in the unit cell, where two sets of four molecules are related by a translation along the longest axis.

Data Collection and Structure Determination

Crystals were quick-soaked in mother liquor supplemented with 15% ethylene glycol, loop mounted, and flash-frozen in liquid nitrogen. In all cases, data were collected at the selenium anomalous edge. Data for Efr3-N were collected at NSLS beamline X29, and data for Ypp1-N and $Ypp1_{11–817(\Delta 732–741)}$ were collected at the NE-CAT beamline 24ID-E at Advanced Photon Source (APS). The data were integrated and scaled using HKL2000 and Scalepack (Otwinowski and Minor, 1997) (Table 1).

Structures for Efr3-N and Ypp1-N were solved by the SAD method (Hendrickson and Ogata, 1997) at 3.2 Å and 3.0 Å resolution, respectively. Selenium positions were located using SHELX (Sheldrick, 2008), and we used SHARP (Vonrhein et al., 2007) to calculate phases and for solvent flattening. Representative electron density for Efr3-N is shown (Figure S1A). We built models for Efr3-N and Ypp1-N using COOT (Emsley and Cowtan, 2004), and we refined the model for Efr3-N in PHENIX (Adams et al., 2002), using torsion angle dynamic, real space, positional, translation/libration/screwmotion, and individual B-factor refinement options and secondary structure restraints (Table 1). We did not refine the Ypp1-N model and used the unrefined structure as a molecular replacement model for phasing the $Ypp1_{11–817(\Delta 732–741)}$ structure.

For molecular replacement, we used Phaser (McCoy, 2007), positioning eight copies of Ypp1-N in the $Ypp1_{11–817(\Delta 732–741)}$ crystal. We identified selenium sites using the MR-SAD option in Phaser, as implemented in PHENIX (Adams et al., 2002), and combined phase information from the partial model (Ypp1-N) with phases obtained by SAD. The electron density maps were further improved by noncrystallographic symmetry (NCS) averaging either in PHENIX (Adams et al., 2002) or else in DM (K. Cowtan, 1994, CCP4 Newsletter on Protein Crystallography). Based on these maps (representative density is shown in Figure S1B), we were able to build additional portions of Ypp1. Several cycles of MR-SAD phase combination, NCS averaging, and model building were required to finally identify 101 of 136 possible selenium positions and to build the entire Ypp1 molecule. The model of Ypp1 was refined in PHENIX similarly to Efr3-N (Table 1) but using NCS restraints.

We used Consurf for conservation analysis (Ashkenazy et al., 2010), Pymol for rendering structure figures (W.L DeLano, PyMOL molecular graphics system [Schrodinger]), and GRASP to calculate electrostatic surface potential (Nicholls et al., 1991).

Liposome Binding Assays

We made liposomes by suspending lipids (Avanti Polar Lipids; Echelon) in buffer (20 mM Tris [pH 7.4 at 21 °C], 150 mM NaCl, and 1 mM TCEP) and vortexing vigorously. We incubated 100 μg of liposomes with 10 μg protein in buffer (20 mM Tris [pH 7.4 at 21 °C], 150 mM NaCl, 1 mM TCEP, and 10% glycerol) for 15 min at room temperature. The incubation mixture was then diluted to 2.5% glycerol by adding an equal volume of glycerol-free buffer (20 mM Tris [pH 7.4 at 21 °C], 150 mM NaCl, and 1 mM TCEP), allowing sedimentation of liposomes. Liposomes were sedimented by centrifugation at 16,000 g for 15 min at 4°C. Protein in the supernatant and the pellet was analyzed by SDS-

PAGE electrophoresis, visualized by staining with Coomassie blue, and quantitated using ImageJ (Abramoff et al., 2004).

Size-Exclusion Chromatography with Ypp1 and Stt4

Hexahistidine-tagged Ypp1 was purified by affinity chromatography and gel filtration, as described for the Ypp1 crystallization construct. FLAG-tagged Stt4 was expressed in HEK293T cells and the cells lysed by suspension in binding buffer (20 mM HEPES [pH 7.4], 150 mM NaCl, 1 mM TCEP, 1% Triton-X, and protease inhibitor). Cleared cell lysate was applied to ANTI-FLAG affinity resin (Sigma) and eluted using 3×FLAG peptide (Sigma) in elution buffer (20 mM HEPES [pH 7.4] and 150 mM NaCl). After elution 1 mM TCEP and protease inhibitors were added.

His_6-Ypp1 and FLAG-Stt4 were individually analyzed by gel filtration (Super-de×200 10/300; GE Healthcare) in gel filtration buffer (20 mM HEPES [pH 7.4], 150 mM NaCl, 1mM TCEP, and protease inhibitor). The mixture of His_6-Ypp1 and FLAG-Stt4 was incubated at 4°C for ~2 hr before the sample was applied to the same gel filtration column. The fractions were analyzed by SDS-PAGE and western blotting using anti-FLAG (Sigma) or anti-HIS antibodies (Sigma).

Protein-Protein Interaction Studies with Ypp1 and Stt4

FLAG-tagged Stt4 was expressed in HEK293T cells by transfection with Lipofectamine (Invitrogen) according to the manufacturer's protocol. The cells were lysed by suspension in binding buffer. GST and GST-tagged Ypp1 constructs were immobilized on glutathione-S-Sepharose beads, which were added to the Stt4-containing HEK293T cell lysate for 1 hr of incubation at 4°C. The resin was washed three times with binding buffer. Proteins were eluted with SDS sample buffer and analyzed by SDS-PAGE and western blotting with anti-FLAG antibody (Sigma).

Protein-Protein Interaction Studies with Ypp1 and Efr3-C

GST-tagged fragments of Efr3 or mutated versions (S684E/S687E and T687E/T690E) were incubated with Ypp1, or fragments thereof, in binding buffer at 4°C for 1 hr. After addition of glutathione-S-Sepharose resin (10–15 μl; GE Healthcare), the mixture was incubated for an additional hour at 4°C, and then washed three times with binding buffer. Bound proteins were eluted from the beads by SDS sample buffer and analyzed by SDS-PAGE and Coomassie blue staining.

Yeast Strains

Yeast strains in which endogenous Efr3 was replaced by Efr3 mutants or wild-type Efr3 were generated by the plasmid shuffling method (Sikorski and Boeke, 1991). Briefly, strains BY4741 and BY4742 were mated to generate a heterozygous diploid strain. The heterozygous diploid EFR3/efr3Δ::KanMX strain carrying the pRS416EFR3 (CEN-URA) plasmid was sporulated and dissected to obtain a haploid efr3Δ::KanMX strain complemented by plasmid. Then, pRS415 (CEN-LEU) plasmids carrying either wild-type Efr3, Efr3-GFP, or mutant versions were transformed into haploid cells, and the CEN-URA

plasmids were removed by selecting transformed cells on 5-fluoroorotic acid (5-FOA) plates at 30°C.

GFP-Stt4 was expressed against the Efr3 background using the pRS416 vector.

Efr3 and Ypp1 constructs similar to those introduced into yeast were recombinantly expressed and purified from *E. coli* and characterized in vitro. Efr3-3-$N_{8–562}$ (K12A, R46D, K49A, K52A, H67E, and R69A), Ypp1-δ$N_{11–817}$ (F255A, F303A, Q304A, and N342A), Ypp1 (11–725), Ypp1 (11–446) migrated as monomers as assessed by gel filtration and are well folded and primarily α helical as assessed by circular dichroism (Figure S2). Efr3-4-$N_{8–562}$ (V292D, Y296A, S336K, D339A, K371A, and D380A) and Ypp1 (11–805) were prone to aggregation, migrating in the void volume of the sizing column (Superdex 200; GE Healthcare).

Metabolic Labeling

Analysis of cellular phosphoinositide levels was carried out as in Nakatsu et al. (2012). Briefly, cells in log phase were collected and incubated in inositol-free medium supplemented with [^{3}H] myo-inositol (Perkin Elmer) at 38°C for 1 hr. Lipid was extracted and loaded onto a Shimadzu Ultrafast Liquid Chromatograph coupled to a Beta-RAM RHPLC detector (LabLogic). The identity of each peak was determined by comparison to known compounds, and the levels of PI3P, PI4P, and PI(4,5)P_2 reported are as a percentage of total detectable inositol phospholipid.

Live-Cell Imaging, Yeast

Cells were grown to log phase (OD_{600} = 0.6), concentrated, and mounted on a microscope slide in synthetic media. Three-dimensional image stacks were collected in 0.3 μ z increments on a DeltaVision Elite workstation (Applied Precission Instruments) based on an inverted microscope (IX-70; Olympus) using a 100×, 1.4 NA oil immersion lens. Images were captured at room temperature (24°C) with a 12-bit charge-coupled-device camera (CoolSnap HQ; Photometrics) and deconvolved using the iterative-constrained algorithm and the measured point spread function.

Cortical patch to cytosol intensity ratio and patch density analysis were carried out as described (Chi et al., 2012). Briefly, the medial z plane from 3D image stacks of large budded cells was used to identify the brightest cortical patch in a cell, and the intensity of the brightest pixel was divided by fluorescence from the cell cytosol. A representative background intensity value (outside the cell) was also subtracted from both patch and cytosolic intensities before calculating the patch/cytosol ratio (n = 30 cells for each strain). Patch densities (patches/surface area in μm^2) were calculated using optical z sections and shown as max projections (n = 30 for each strain). All images, 3D graphs, and data analysis were acquired using Delta Vision Soft-WoR× 5.5 software.

Live-Cell Imaging, Mammalian Cells

HeLa cells were cotransfected with mRFP-FYVE (Hrs) (obtained from H. Stenmark, Oslo University, Oslo, Norway) and either wild-type EFR3A-GFP (Nakatsu et al., 2012) or a

quintuple basic site mutant of EFR3A-GFP (K50E/R53A/R61E/R68E/R70E). Twenty-four hours after transfection (using FuGENE HD according to the manufacturer's instructions; Promega), live cells were imaged on an UltraVIEW VoX spinning-disc confocal microscope system (Per-kinElmer) including aninverted microscope (Ti-E Eclipse; Nikon) equipped with Perfect Focus, temperature-controlled stage, 14-bit electron-multiplying charge-coupled-device camera (C9100-50; Hamamatsu Photonics) and spinning disc-confocal scan head (CSU-X1; Yokogawa Corporation of America) controlled by Volocity software (PerkinElmer). Images were acquired through a 100× oil objective (1.4 NA; CFI Plan Apochromat VC). Green fluorescence was excited with a 488 nm/50 mW diode laser (Coherent) and collected by a band pass (BP) 527/55 nm filter. Red fluorescence was excited with a 561 nm/50 mW diode laser (Cobolt) and collected by a BP 615/70 nm filter. Multicolor images were acquired sequentially.

The basic site mutant of EFR3A-GFP (K50E/R53A/R61E/R68E/R70E) was generated from wild-type EFR3A-GFP (Nakatsu et al., 2012) using three sequential rounds of site-directed mutagenesis (QuikChange II XL; Agilent Technologies).

Supplementary Material

Refer to Web version on PubMed Central for supplementary material.

Acknowledgments

We are grateful to the staffs at NE-CAT beamline 24ID-E at the APS and X29 at NSLS for assistance with data collection. We thank Fubito Nakatsu and Michelle Pirrucello for helpful discussions during the course of these studies. This work was supported by the NIH (GM080616 to K.M.R., GM095766 to C.G.B., and R37NS36251 to P.D.C.) and by grants from the Simons Foundation and the Yale Center for Genomics and Proteomics (P30DA018343) to P.D.C. J.M.B. is a recipient of a Jane Coffin Childs fellowship.

References

Abramoff MD, Magalhães PJ, Ram SJ. Image processing with ImageJ. Biophotonics International. 2004; 11:36–42.

Adams PD, Grosse-Kunstleve RW, Hung LW, Ioerger TR, McCoy AJ, Moriarty NW, Read RJ, Sacchettini JC, Sauter NK, Terwilliger TC. PHENIX: building new software for automated crystallographic structure determination. Acta Crystallogr D Biol Crystallogr. 2002; 58:1948–1954. [PubMed: 12393927]

Altan-Bonnet N, Balla T. Phosphatidylinositol 4-kinases: hostages harnessed to build panviral replication platforms. Trends Biochem Sci. 2012; 37:293–302. [PubMed: 22633842]

Ashkenazy H, Erez E, Martz E, Pupko T, Ben-Tal N. ConSurf 2010: calculating evolutionary conservation in sequence and structure of proteins and nucleic acids. Nucleic Acids Res. 2010; 38:W529–W533. Web Server issue. [PubMed: 20478830]

Audhya A, Emr SD. Stt4 PI 4-kinase localizes to the plasma membrane and functions in the Pkc1-mediated MAP kinase cascade. Dev Cell. 2002; 2:593–605. [PubMed: 12015967]

Audhya A, Foti M, Emr SD. Distinct roles for the yeast phospha-tidylinositol 4-kinases, Stt4p and Pik1p, in secretion, cell growth, and organelle membrane dynamics. Mol Biol Cell. 2000; 11:2673–2689. [PubMed: 10930462]

Balla A, Balla T. Phosphatidylinositol 4-kinases: old enzymes with emerging functions. Trends Cell Biol. 2006; 16:351–361. [PubMed: 16793271]

Baird D, Stefan C, Audhya A, Weys S, Emr SD. Assembly of the PtdIns 4-kinase Stt4 complex at the plasma membrane requires Ypp1 and Efr3. J Cell Biol. 2008; 183:1061–1074. [PubMed: 19075114]

Chi RJ, Torres OT, Segarra VA, Lansley T, Chang JS, Newpher TM, Lemmon SK. Role of Scd5, a protein phosphatase-1 targeting protein, in phosphoregulation of Sla1 during endocytosis. J Cell Sci. 2012; 125:4728–4739. [PubMed: 22825870]

Conti E, Müller CW, Stewart M. Karyopherin flexibility in nucle-ocytoplasmic transport. Curr Opin Struct Biol. 2006; 16:237–244. [PubMed: 16567089]

D'Angelo G, Vicinanza M, Di Campli A, De Matteis MA. The multiple roles of PtdIns(4)P — not just the precursor of PtdIns(4,5)P_2. J Cell Sci. 2008; 121:1955–1963. [PubMed: 18525025]

Di Paolo G, De Camilli P. Phosphoinositides in cell regulation and membrane dynamics. Nature. 2006; 443:651–657. [PubMed: 17035995]

Doublie, S. Preparation of selenomethionyl proteins for phase determination. In: Carter, CW.; Sweet, RM., editors. Methods in Enzymology: Macromolecular Crystallography. New York: Academic Press; 1997. p. 523-530.

Emsley P, Cowtan K. Coot: model-building tools for molecular graphics. Acta Crystallogr D Biol Crystallogr. 2004; 60:2126–2132. [PubMed: 15572765]

Foti M, Audhya A, Emr SD. Sac1 lipid phosphatase and Stt4 phosphatidylinositol 4-kinase regulate a pool of phosphatidylinositol 4-phosphate that functions in the control of the actin cytoskeleton and vacuole morphology. Mol Biol Cell. 2001; 12:2396–2411. [PubMed: 11514624]

Hendrickson, WA.; Ogata, CM. Phase determination from multi-wavelength anomalous diffraction methods. In: Carter, CW.; Sweet, RM., editors. Methods in Enzymology: Macromolecular Crystallography. New York: Academic Press; 1997. p. 494-523.

Huang FD, Matthies HJ, Speese SD, Smith MA, Broadie K. Rolling blackout, a newly identified PIP2-DAG pathway lipase required for Drosophila phototransduction. Nat Neurosci. 2004; 7:1070–1078. [PubMed: 15361878]

Jesch SA, Gaspar ML, Stefan CJ, Aregullin MA, Henry SA. Interruption of inositol sphingolipid synthesis triggers Stt4p-dependent protein kinase C signaling. J Biol Chem. 2010; 285:41947–41960. [PubMed: 20972263]

McCoy AJ. Solving structures of protein complexes by molecular replacement with Phaser. Acta Crystallogr D Biol Crystallogr. 2007; 63:32–41. [PubMed: 17164524]

Misra S, Puertollano R, Kato Y, Bonifacino JS, Hurley JH. Structural basis for acidic-cluster-dileucine sorting-signal recognition by VHS domains. Nature. 2002; 415:933–937. [PubMed: 11859375]

Muhua L, Adames NR, Murphy MD, Shields CR, Cooper JA. A cytokinesis checkpoint requiring the yeast homologue of an APC-binding protein. Nature. 1998; 393:487–491. [PubMed: 9624007]

Nakatsu F, Baskin JM, Chung J, Tanner LB, Shui G, Lee SY, Pirruccello M, Hao M, Ingolia NT, Wenk MR, et al. PtdIns4P synthesis by PI4KIIIα at the plasma membrane and its impact on plasma membrane identity. J Cell Biol. 2012; 199:1003–1016. [PubMed: 23229899]

Nicholls A, Sharp KA, Honig B. Protein folding and association: insights from the interfacial and thermodynamic properties of hydrocarbons. Proteins. 1991; 11:281–296. [PubMed: 1758883]

Otwinowski, Z.; Minor, W. Processing of X-ray diffraction data collected in oscillation mode. In: Carter, CW.; Sweet, RM., editors. Macromolecular Crystallography. New York: Academic Press; 1997. p. 307-326.

Reiss S, Rebhan I, Backes P, Romero-Brey I, Erfle H, Matula P, Kaderali L, Poenisch M, Blankenburg H, Hiet MS, et al. Recruitment and activation of a lipid kinase by hepatitis C virus NS5A is essential for integrity of the membranous replication compartment. Cell Host Microbe. 2011; 9:32–45. [PubMed: 21238945]

Sheldrick GM. A short history of SHELX. Acta Crystallogr A. 2008; 64:112–122. [PubMed: 18156677]

Shiba T, Takatsu H, Nogi T, Matsugaki N, Kawasaki M, Igarashi N, Suzuki M, Kato R, Earnest T, Nakayama K, Wakatsuki S. Structural basis for recognition of acidic-cluster dileucine sequence by GGA1. Nature. 2002; 415:937–941. [PubMed: 11859376]

Sikorski, RS.; Boeke, JD. In vitro mutagenesis and plasmid shuffling: from cloned gene to mutant yeast. In: Abelson, JN.; Simon, MI.; Guthrie, C.; Fink, GR., editors. Methods in Enzymology. New York: Academic Press; 1991.

Tabuchi M, Audhya A, Parsons AB, Boone C, Emr SD. The phosphatidylinositol 4,5-biphosphate and TORC2 binding proteins Slm1 and Slm2 function in sphingolipid regulation. Mol Cell Biol. 2006; 26:5861–5875. [PubMed: 16847337]

Trotter PJ, Wu WI, Pedretti J, Yates R, Voelker DR. A genetic screen for aminophospholipid transport mutants identifies the phosphatidylinositol 4-kinase, STT4p, as an essential component in phosphatidylserine metabolism. J Biol Chem. 1998; 273:13189–13196. [PubMed: 9582361]

Vonrhein C, Blanc E, Roversi P, Bricogne G. Automated structure solution with autoSHARP. Methods Mol Biol. 2007; 364:215–230. [PubMed: 17172768]

Yoshida S, Ohya Y, Nakano A, Anraku Y. Genetic interactions among genes involved in the STT4-PKC1 pathway of Saccharomyces cerevisiae. Mol Gen Genet. 1994; 242:631–640. [PubMed: 8152413]

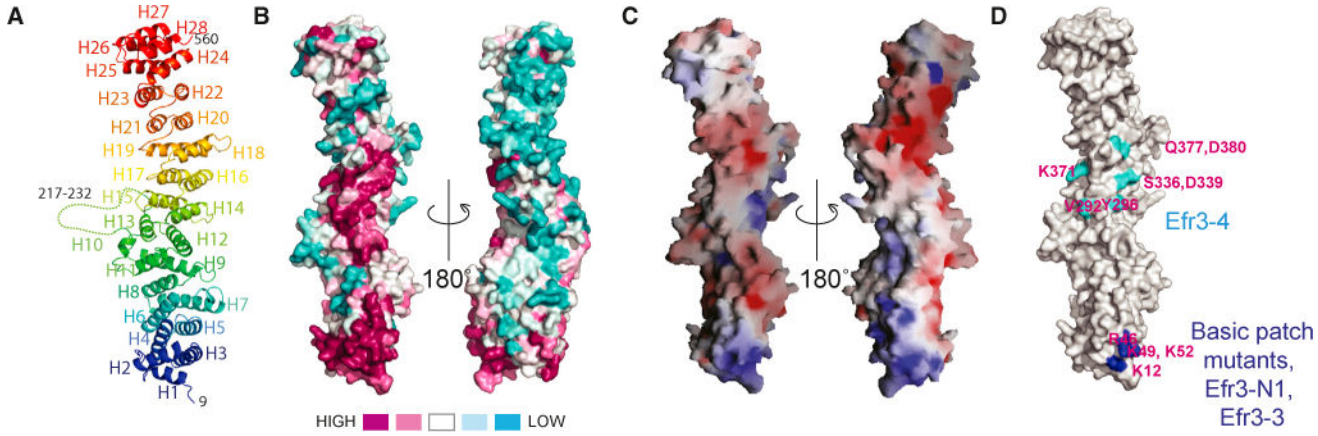

Figure 1. Structure of Efr3-N

(A) Ribbons diagram, colored blue to red from N terminus to C terminus.

(B) Conservation in Efr3-N. Orientation at left is as in (A). Surfaces around the N terminus of Efr3-N and in the middle of the rod are highly conserved.

(C) Electrostatic potential. The conserved surface at the N terminus is basic.

(D) Location of mutations mapped onto structure. Residues H67 and R69, which are mutated in Efr3-3 and Efr3-N2, are in the conserved basic patch, but not visible here. Recombinant Efr3-3 is well folded as assessed by CD (Figure S2), but Efr3-4 aggregates in vitro.

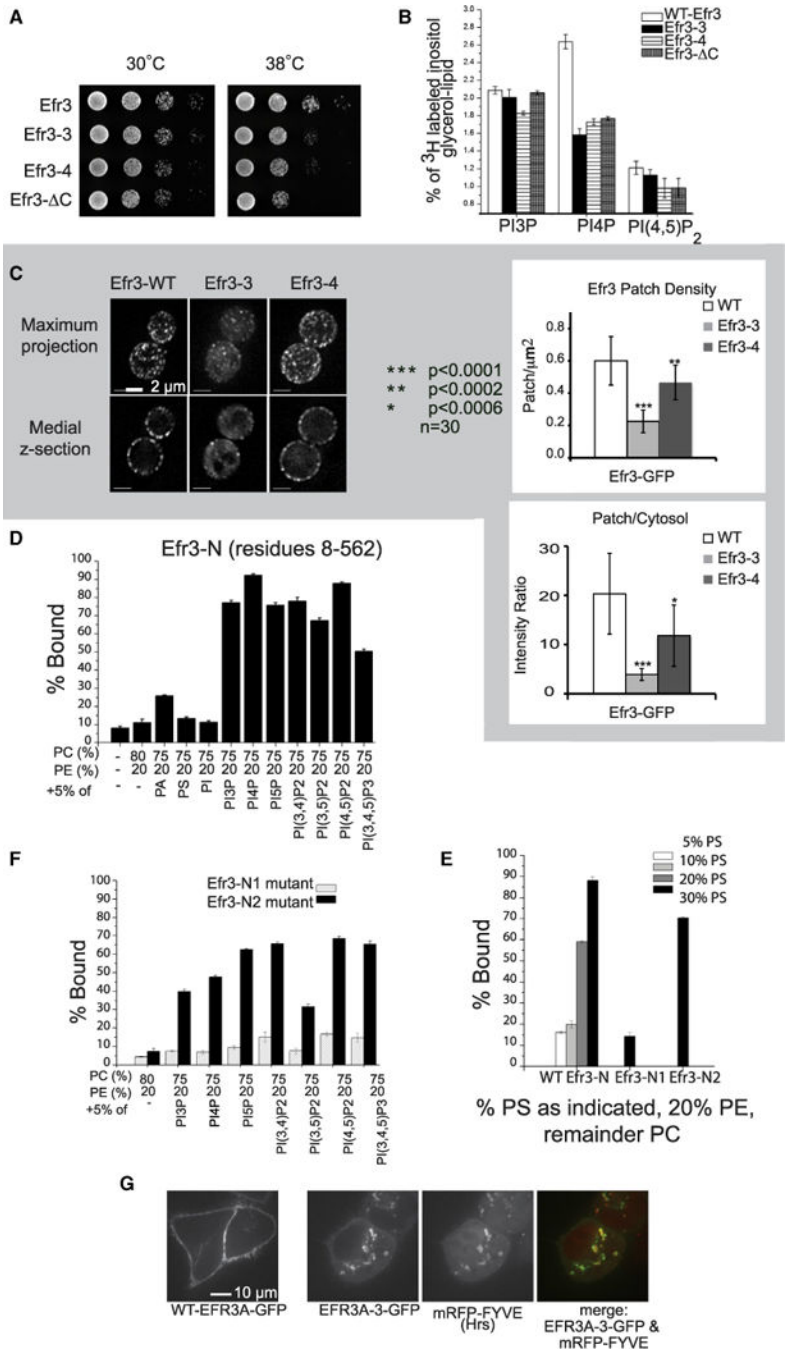

Figure 2. Conserved Surfaces in Efr3-N Are Important for Function

(A) Yeast strains with Efr3 mutants are growth impaired as compared to those with wild-type protein.

(B) Cellular phosphoinositide levels in wild-type and Efr3 mutant strains. PI4P levels are reduced by 30%–40% in the Efr3-3, Efr3-4, and Efr3-ΔC mutants. Error bars are SD.

(C) Localization of Efr3-GFP constructs in yeast and quantitation. Membrane localization is reduced for Efr3-3, which has mutations in the conserved basic patch. Student's t test was used to calculate p values.

(D) Liposome binding assays. Experiments shown are sedimentation assays carried out in triplicate; error bars represent SD. Efr3 associates with phosphoinositide-containing liposomes, though nonspecifically. Similar results were obtained using flotation assays (Figure S3).

(E) Efr3 also associates with liposomes containing phosphatidylserine, which comprises ~30% of the plasma membrane. Binding is reduced in Efr3-N1 when residues (K12A, R46D, K49A, and K52A) in the conserved basic patch are mutated, but not in Efr3-N2, in which a different and smaller subset of basic patch residues (H67E and R69A) is altered.

(F) Binding to phosphoinositide-containing liposomes is significantly reduced for Efr3-N, 1 but not Efr3-N2.

(G) Murine EFR3A-GFP and the basic-patch mutant EFR3A-3-GFP were expressed in HeLa cells. EFR3A-3 colocalizes with the endosomal/lysosomal marker mRFP-Fyve and does not go to the plasma membrane like wild-type protein.

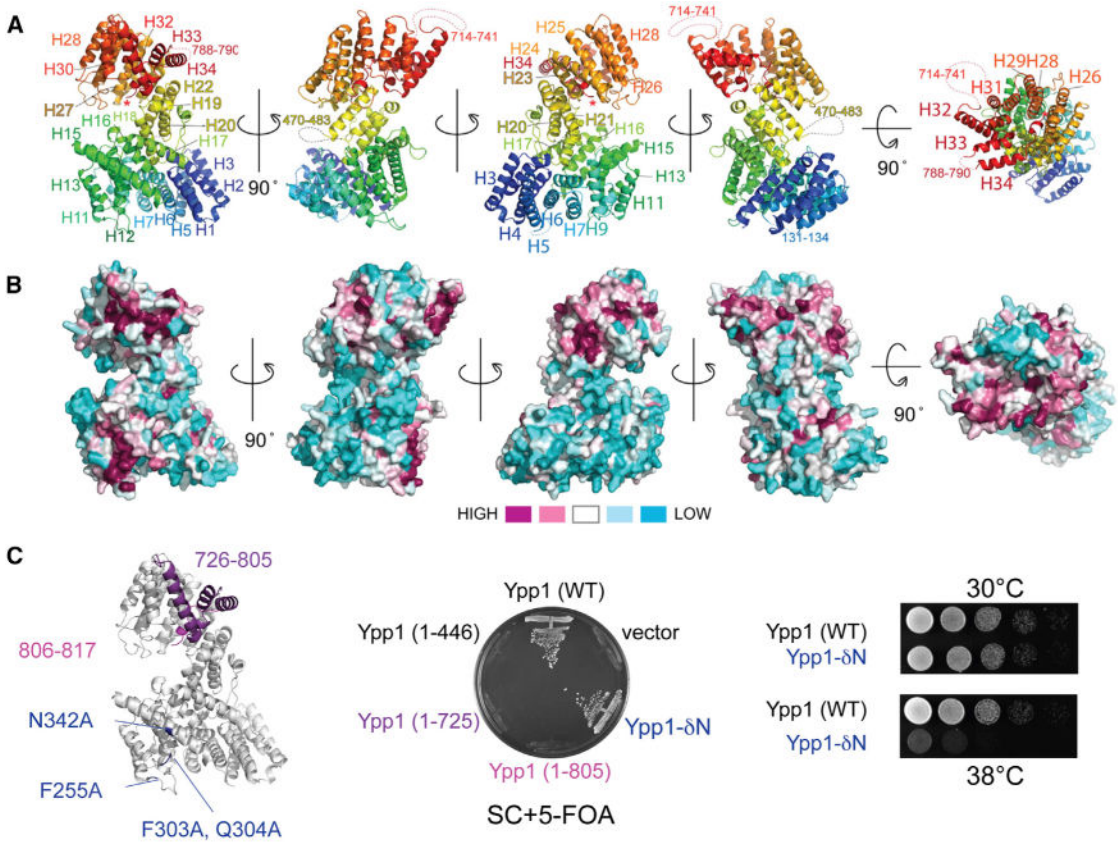

Figure 3. Ypp1 Is a HEAT-Repeat Superhelix

(A) Ribbons diagram, colored blue to red from the N terminus to the C terminus. The very C terminus is inserted into the center of the Ypp1 spiral and is marked with *. See also Figure S4.

(B) Surface conservation, with orientation as in (A).

(C) At left, C-terminal deletions in Ypp1 and residues that were mutated in Ypp1-δN are indicated. In middle, wild-type Ypp1 and Ypp1-δN, but not C-terminally truncated Ypp1 constructs, can rescue Ypp1 null yeast strains. At right, Ypp1-δN has a growth defect at restricted temperature. (See Figure S2 for CD profiles of Ypp1 mutants.)

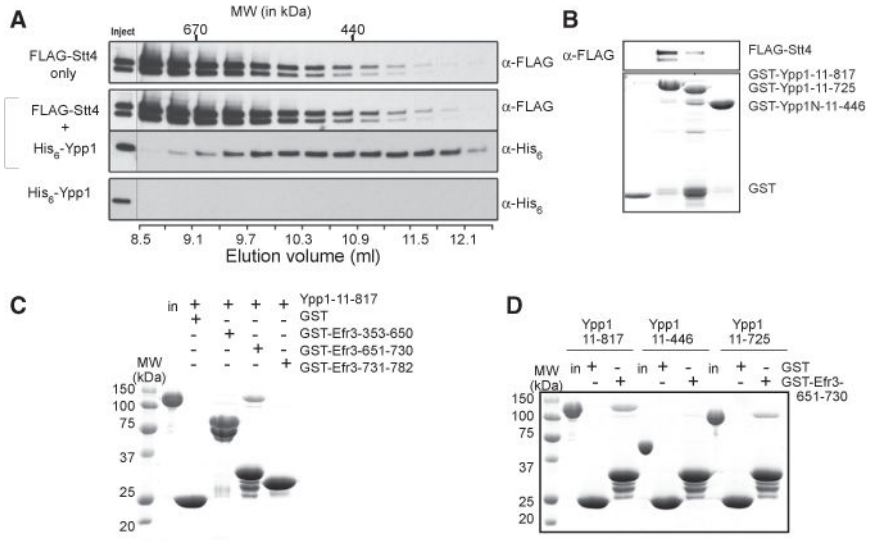

Figure 4. The C-Terminal Portion of Ypp1 Is Required for Interactions with Stt4 and Efr3

(A) Gel filtration chromatography (Superdex200 10/300) showing elution profiles of affinity-purified FLAG-Stt4 (top panel), His6-Ypp1 (bottom panel), and a mixture of FLAG-Stt4 and His6-Ypp1 (middle panels). Stt4 is partially aggregated and mostly in the void volume, with only a small monodisperse fraction. Ypp1 alone elutes at 13.75 ml. Its elution peak shifts in the presence of Stt4, and Ypp1 comigrates with monodisperse Stt4. They elute at 10.8 ml, similarly to the ~440 kDa ferritin calibration standard. The column was calibrated with HMW calibration standards (Biorad) and ferritin (Sigma).

(B) Pull-down of recombinant FLAG-tagged Stt4 by purified Ypp1 constructs. Stt4 interacts with fragments that include C-terminal portions of Ypp1 and not with the N-terminal half of Ypp1.

(C) Pull-down of Ypp1 by C-terminal fragments of Efr3. Ypp1 interacts with an Efr3 fragment including residues 651–730.

(D) Pull-down of Ypp1 constructs by an Efr3 C-terminal fragment. Only fragments that include C-terminal portions of Ypp1 interact with Efr3; Ypp1-N does not.

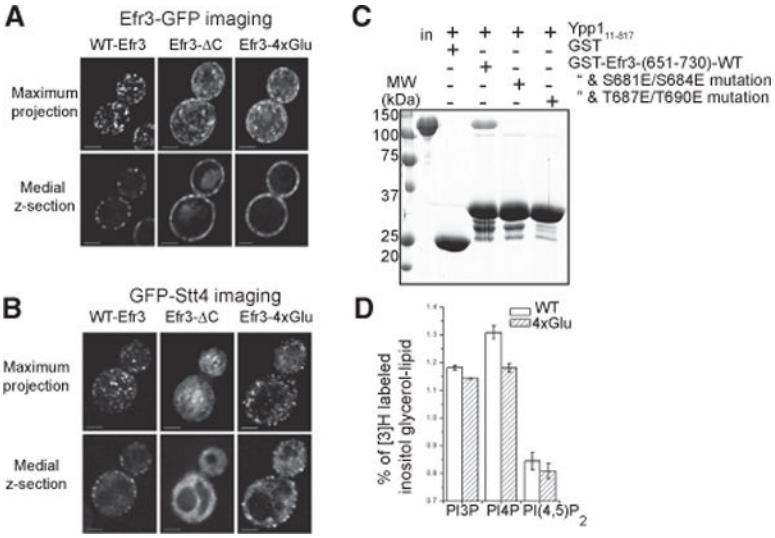

Figure 5. Efr3 C-Terminal Phosphorylation Modulates the Efr3-Ypp1 Interaction and Stt4 Complex Assembly

(A) Efr3-ΔC-GFP localizes to the plasma membrane in yeast, but does not form *punctae* like wild-type Efr3-GFP. The Efr3-4×Glu mutant has a similar phenotype.

(B) GFP-Stt4 is mostly cytosolic when expressed in a Efr3-ΔC background and does not localize to the plasma membrane. Stt4-GFP plasma membrane localization is also reduced in the Efr3-4×Glu background.

(C) Ypp1 pull-down with C-terminal fragments of Efr3 (residues 651–730). Mutating S681/S684 or T687/T690 to glutamate to mimic their phosphorylation reduced the interaction between Ypp1 and Efr3.

(D) Cellular PI4P levels are reduced by ~10% in yeast strains with Efr3-4×Glu as compared to wild-type protein.

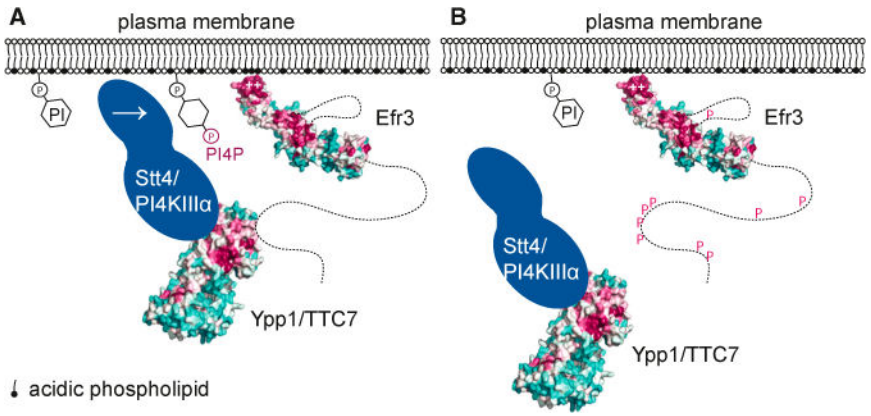

Figure 6. Stt4/PI4KIIIα Targeting to the Plasma Membrane

(A) A conserved basic patch at the N-terminal end of Efr3 mediates complex association with the plasma membrane. The Efr3 C terminus and Stt4/PI4KIIIα both interact with the C-terminal portion of Ypp1. As yet, no function has been assigned to conserved surfaces at the middle of Efr3-N or in the Ypp1 N-terminal half.

(B) Stt4/PI4KIIIα recruitment to the plasma membrane is reduced when the Efr3 C terminus is phosphorylated to interrupt the Efr3-Ypp1 interaction. P indicates that the Efr3 C terminus is heavily phosphorylated in vivo.

Table 1

Data Collection and Refinement Statistics

	Efr3(8–562)	Ypp(11–817)	Ypp(11–446)
Data Collection			
Heavy atom	Se	Se	Se
Space group	P 6_4 22	P1	P 2_1 2_1 2_1
Unit cell dimensions (a, b, c in Å; α, β, γ in °)	136.374, 136.374, 141.143, 90, 90, 120	97.545, 136.65, 154.125, 76.689, 85.673, 72.744	102.345, 129.202, 185.452, 90, 90, 90
Wavelength (Å)	0.9792	0.9792	0.9792
Resolution (Å)	29.53–3.20 (3.31–3.20)	25.0–3.25 (3.37–3.25)	30.0–3.04 (3.17–3.04)
R_{merge} (%)[a]	10.5 (69.1)	11.2 (58.2)	17.3 (77.8)
I/σ	23.0 (2.7)	9.2 (1.4)	18.1 (3.9)
Completeness (%)	99.4 (100.0)	98.8 (98.7)	100.0 (100.0)
Redundancy	14.3 (14.3)	2.0 (2.0)	13.5 (13.7)
Refinement			
Resolution (Å)	29.53–3.20	25.1–3.25	–
No. of unique reflections	13,197	114,694	–
R_{work}/R_{free} (%)[b]	23.11/25.56	23.98/27.72[c]	–
No. of protein atoms	4,326	48,674	–
Average B (Å^2)	103.83	79.19	–
Rmsd			
Bond length (Å)	0.004	0.004	–
Bond angle (°)	0.738	0.944	–
Ramachandran plot[d]			
Allowed (% residues)	95.8	97.3	–
Generously allowed (% residues)	4.0	2.6	–
Disallowed (% residues)	0.2	0.1	–

Numbers in parentheses represent values in the highest resolution shell. See Figure S1 for representative electron density maps.

[a] $R_{merge} = \sum_h \sum_i \left| I_{(h)i} - \langle I_{(h)} \rangle \right| / \sum_h \sum_i I_{(h)I}$.

[b] $R_{merge} = \sum_h |F_{obs} - F_{calc}| / \sum_h F_{obs}$.

[c] R_{free} set was chosen by the thin shell method to avoid NCS bias.

[d] As defined by Molprobity.